Comparative Analysis and Joint Inversion of MT and ZTEM Data

Wolfgang Soyer*
CGG Multi-Physics Imaging
Milan, Italy
wolfgang.soyer@cgg.com

Randall Mackie
CGG Multi-Physics Imaging
Milan, Italy
randall.mackie@cgg.com

SUMMARY

Ground Magnetotelluric (MT) data acquired today are typically broadband, covering 0.001 to >1000 Hz with inter-site spacing typically at 500 to 1000 m. Airborne Z-axis tipper data (ZTEM) are sampled at higher spatial density but usually band-limited to frequencies >30Hz. We analyze a pair of overlapping 3D surveys to examine lateral and vertical spatial sensitivity.

The MT data include a 2D line and a 3D survey. The line data also has magnetic tipper data that allows for a direct comparison with ZTEM; in the overlapping frequency range the agreement between the two magnetic data sets is good, with ZTEM showing higher lateral smoothness.

CGG's RLM-3D non-linear conjugate gradient MT-CSEM inversion engine was extended to accurately model the ZTEM data, using measured sensor altimetry data and detailed 3D topography. Both single domain and joint inversions of the ZTEM and MT data were carried out. A suite of inversions were run to test the influence of starting resistivity and regularization parameters on output models, equally for MT, ZTEM, and joint MT+ZTEM inversions to allow for direct comparison.

ZTEM single domain inversion results depend strongly on the starting resistivity value, confirming that the method maps relative variations rather than absolute resistivity values, as expected for magnetics-only measurements. Shallower lateral structure shows qualitative agreement with the MT, but at depth resistivity from ZTEM inversion is driven by model regularization only. Joint inversion improved the relatively shallow section, calibrating the ZTEM resistivities and adding continuity between the MT sites. Below around 1000m depth, the 3D resistivity model is controlled by the MT data alone. Our overall conclusion is that today's 3D broadband MT only benefits from joint MT-ZTEM acquisition and inversion workflows in the case of sparse MT station spacing.

Key words: MT, ZTEM, 3D joint inversion.

INTRODUCTION

Magnetotelluric and airborne ZTEM are both inductive passive EM methods, where source signals are assumed to be uniform over the area of a survey. In the frequency overlap covered by both methods – here 30-720Hz – sources originate primarily from distant ("atmospherics"), while for MT frequencies below 1Hz (deeper looking) they relate to ionospheric currents due to fluctuations of solar radiation. Since the source fields are locally uniform in either case, no knowledge on sources is technically required, and therefore the only noticeable difference in numeric modeling of MT and ZTEM is in the sensors location: above versus on ground, and local (MT) versus inter-station (ZTEM) transfer functions.

The characteristics of the two data types however have significant differences, with consequences on their suitability to explore specific targets:

- Local electromagnetic impedances (MT) versus inter-station magnetic transfer functions (ZTEM)
- Coverage of a wide frequency band: typically 0.001-10000 Hz (MT) versus only 30-720 Hz (ZTEM).
- Measurement at comparably few locations (MT) versus almost continuous measurement along flight lines (ZTEM)

To some extent, these qualities can be regarded as complementary: MT impedances provide more absolute subsurface resistivity control with respect to the magnetic-only ZTEM data that sense mostly resistivity variations; ZTEM provides more continuous lateral information; MT impedances are prone to static distortion effects from small scale near-surface structure whereas magnetic transfer functions from ZTEM are not. Most importantly, currents at central and low MT frequencies diffuse at much greater depth.

The two methods have been compared in a number of studies. Agreement of co-located observed datasets was investigated in direct data comparisons (e.g. Hübert et al., 2016, Lee at al., 2017). Single domain inversion results from observed data of both methods were compared in 2D and 3D (e.g., Legault et al., 2012, Hübert et al., 2016). Also joint inversions of the two methods have been performed, both on synthetic and real data sets, using several different inversion codes (**2D**: Wannamaker and Legault, 2014, Alumbaugh et al., 2016; **3D**, Holtham and Oldenburg, 2010, Sasaki et al., 2014, Sattel and Witherly, 2015, Lee et al., 2017). Most authors conclude that the two data types essentially agree and that MT can contribute to an absolute resistivity calibration for ZTEM in a joint analysis, while shallow resistivity variation is mapped in more detail from the contribution of ZTEM.

Here we analyze a co-located MT-ZTEM data set from a mining prospect in Arizona, using the EM component of CGG's RLM-3D nonlinear conjugate gradient (NLCG) engine for single and joint domain inversion workflows, which has been extensively used on

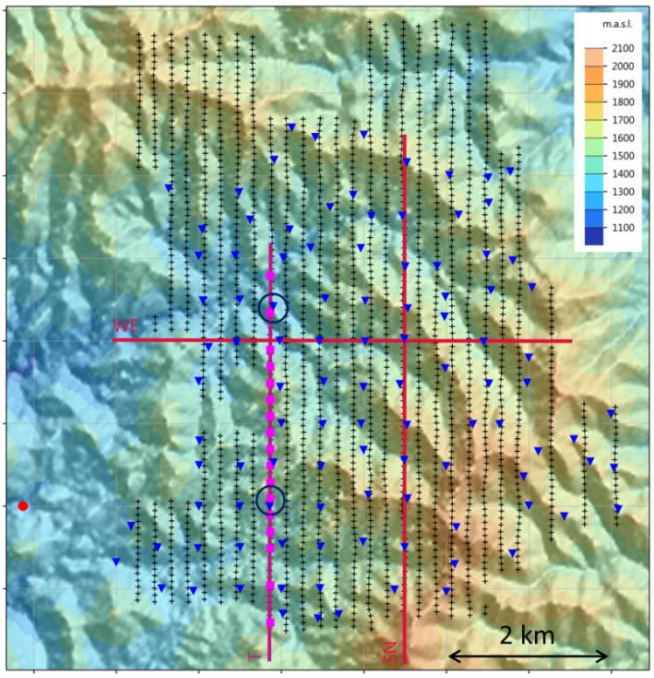

Figure 1: Locations of EM data. Subsampled ZTEM data are shown as black crosses, the location of the horizontal coil pair to the West in red. Pink squares and blue triangles mark MT site locations. Co-located MT data shown in Error! Reference source not found. **are circled**

commercial data sets of multiple geophysical methods (e.g. Soyer et al., 2017) and was extended to model AFMAG / ZTEM (Watts and Mackie, 2012).

The area investigated is of interest for mineral exploration, as intrusive breccia and porphyry deposits have been found close to the study zone. Without alluvium cover except for shallow valley fill, exposed younger Cenozoic volcanics are overlying older igneous Laramide bedrock of the Upper Tertiary. The covering altered volcanics appear to be electrically conductive. Exploration focus is on variations in the resistive basement underneath.

DATA SETS

The roving vertical coil data ("H_z") of the ZTEM method were acquired by Geotech Ltd. along 27 NS flight lines of nominally 200m spacing, covering an area of about 6km by 7km. The fixed horizontal coil pair was installed 1.5km west of the area. Nominal vertical sensor clearance above ground was 80m, but with a nominal flight speed of 22m/s true clearance varied significantly. Data provided are in-phase (real) and quadrature (imaginary) vertical to horizontal magnetic transfer functions for the six frequencies of 30, 45, 90, 180, 360, and 720Hz, plus location information. Original data spacing is about 10m, which was subsampled to about 80m along the lines: data grids are very smooth – smoother than MT tipper data – and have likely undergone considerable filtering or used wide spatial/time windows (details of the processing procedure are not known to the authors). Resolution considerations, also with respect to sensor height and model cell size, further justify the subsampling.

Original ZTEM data were converted from the contractor's coordinate system convention and quadrature polarity and into standard MT transfer function convention using:

$$Tx = -complex(xIP, -xQD)$$
$$Ty = \ \ complex(yIP, -yQD)$$

In agreement with both the description of the acquisition report and comparisons with tipper data along the MT Titan line.

Magnetotelluric data are from two acquisitions by different contractors using different instrumentation:

- 17 sites along a single 4.2 km long NS line at 200m spacing in its center, by Quantec using five-channel Titan systems.
- 106 sites of with 3D coverage by Zonge using their ZEN instruments in a four-channel setup.

Both data sets are broadband, but the Titan data extends to one decade higher frequency to above 10 kHz. The two MT data sets agree well with each other, with the exception that at high frequencies (around 1000Hz) soundings from Zonge data seem less well-defined and may be subject to some bias, as indicated by a direct comparison (Figure 2). Quantec data are noisy in the so-called HF dead band at 2-3000 Hz, but the high quality data above this dead band allows for good judgment of data quality on either side during data editing.

The Titan data set also contains local magnetic tipper data that allow for direct comparison with the airborne data (Figure 3). Quantitative differences are expected between these, due to the different locations of both the vertical and the horizontal magnetic sensors. Considering this, the general agreement between the two tipper data sets is good, however as mentioned ZTEM is considerably smoother in nature. This is likely owing to both noise in MT tipper data and spatial filtering of the ZTEM.

For effective display of induction arrows, ZTEM data were subsampled to about 200m distance. It is noted that the ZTEM transfer functions have a strong correlation with topography particularly at the higher frequencies, with induction arrows pointing uphill, as is typically also observed with MT tipper data sets (e.g. Stark et al, 2013). In fact, MT and

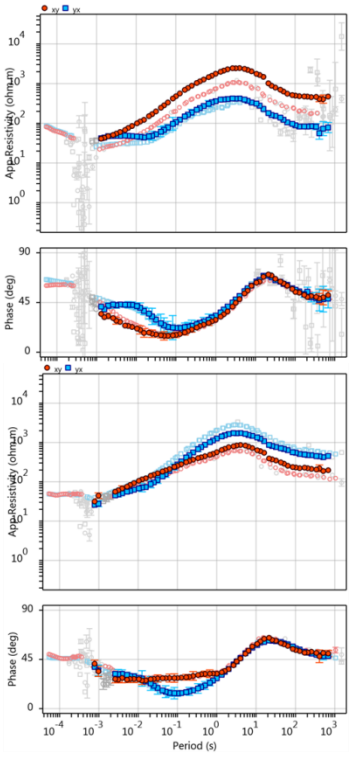

Figure 2: Comparison between nearly co-located Quantec (faint colours) and Zonge data (bold colours, foreground) at two locations. Masked data are in grey. Location of sites is shown in Figure 1.

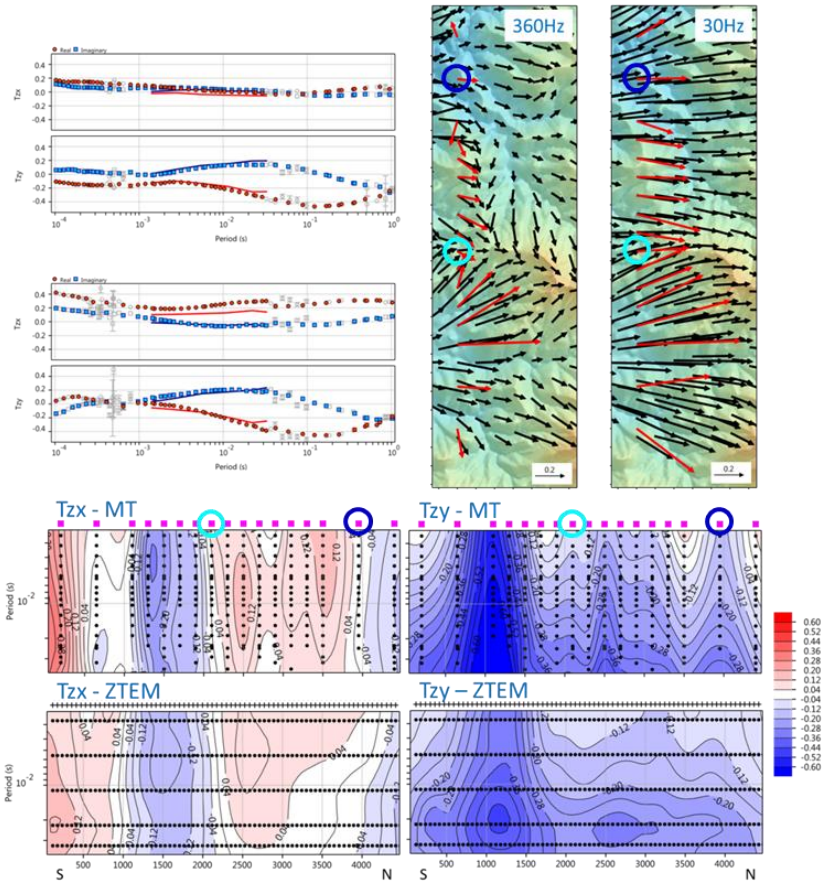

Figure 3: Comparison between nearly co-located MT and ZTEM data tipper data along SN profile "T" (see Figure 1). Sounding plots in two locations (top left; points: MT, line: ZTEM, real parts in red), induction arrows (real parts, top right; MT: red, ZTEM: black) at 30Hz and 360Hz, and pseudo-sections of real parts of tipper (bottom).

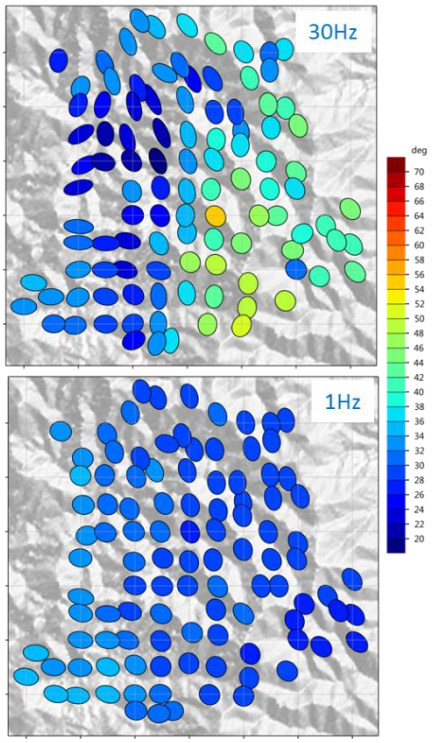

Figure 4: MT phase of the Zonge data set, displayed as ellipses at two frequencies. Color fill is the geometric average of the principal phases.

ZTEM induction arrows show similar trends (Figure 3 and Figure 6), but ZTEM have smoother lateral variation. At the low frequency end of ZTEM (30Hz), the east component of the magnetic transfer function dominates, and indicates lower resistivity to the east.

This is in line with MT impedances at the same frequency: phase tensors (Caldwell, 2014) show higher average phase in the east (Figure 4). With decreasing frequency, phases have low values and are remarkably uniform laterally. This suggests that there's little resistivity variation at deeper levels underneath the shallower conductor.

METHOD AND RESULTS

The MT and ZTEM data sets were inverted both separately and jointly using CGG's RLM-3D NLCG code. This EM inversion algorithm is used routinely on 3D MT data sets for the geothermal, mining and O&G markets (over 100 onshore MT inversion projects in the last 5 years), as well as offshore CSEM data for hydrocarbon exploration. Inversions optionally include gravity or seismic tomography data within a joint workflow using cross-gradients to promote structural similarity between different properties (Soyer et al, 2017).

In order to invert for ZTEM type data, the passive, natural source EM component of the code was extended to handle magnetic sensor data at a specified height above ground. Inter-station transfer functions which are also required to accurately model the observed ZTEM were handled by the code before this modification, because the use of sparse magnetic data at a sub-set of MT sites is common practice, particularly in the mining industry. Inversion in joint 3D modeling is for a single resistivity property on the same 3D mesh. Instead of using a general trade-off parameter as in Lee et al. (2017), data misfit terms for the objective function here are weighted with the inverse of the respective number of data points for each method.

Only the 3D Zonge MT data set was used in the 3D MT inversions, due to their spatial coverage. MT data were inverted in the full available band from 0.0014 Hz to 1,280Hz, using five frequencies per decade. ZTEM were inverted at all six frequencies (30-720Hz). Error floors were 5% for impedances, and a uniform absolute error of 0.012 was assigned to the ZTEM. All 3D inversions were carried out on the same 3D mesh, with 80m lateral cell size in the core, which is similar to the sub-sampled ZTEM data spacing.

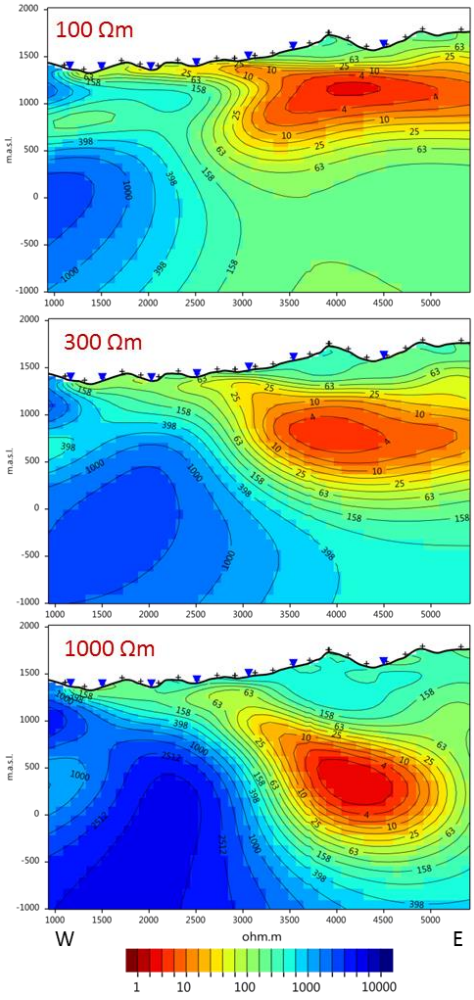

Figure 5: ZTEM 3D inversion results along profile "WE" (Figure 5), for different homogeneous starting resistivities

Vertical cell size is 30m within the topographic range, increasing smoothly to 80m below, again followed by a very subtle increase of 3% per layer down to -8000m msl elevation. Padding of 50 km is added to the core area in all directions.

Single domain ZTEM inversions were performed for different homogeneous starting resistivities: 100, 300, and 1000 Ωm. Data fit was similar in these inversions, with RMS values of 1.40-1.45. Results – here presented along profile "WE" in Figure 5 – show a strong dependence of modelled structure from this starting point, both in terms of absolute resistivity levels and, as a consequence, depth levels of imaged structures. A deep (>1km) low resistivity anomaly as modelled using higher starting values is not in agreement with the observed MT data, and also for 100 Ωm the low resistor still appears to extend to exaggerated depth levels with respect to MT results (Figure 8).

Comparison of single domain and joint inversions shows a rather subtle modification of MT results with the inclusion of the ZTEM data to the inversion procedure. Contrasts however sharpen slightly and continuity of features is somewhat increased in joint inversions. Data misfit in joint inversions did increase with respect to the single domain analysis, but only moderately: 1.30 from 1.28 (MT), and 1.59 from 1.44 (ZTEM), reflected also in comparisons between observed data and calculated responses (Figure 7).

CONCLUSIONS

For the data sets at hand, good general agreement between airborne inter-station magnetic transfer functions (ZTEM) and land-based local tipper was found. As generally the case with magnetic transfer functions at high frequency, ZTEM data show a strong contribution from topography at the higher frequencies. Data variation in ZTEM both laterally and with frequency is very smooth compared to MT, suggesting that considerable spatial filtering may have been applied to the data. The broadband MT data used in 3D inversions are local electromagnetic impedances only. These extend to only slightly higher frequency than ZTEM, and there are indications of noise at the high frequency end. MT data show only minor lateral variation below the ZTEM frequency band.

There are theoretical considerations on perfect, continuous data sets that might draw a more encouraging picture regarding the non-uniqueness of tipper only inversions (Soyer, 2002). Practically however, the 3D inversions performed here demonstrate that ZTEM – like any tipper data method – can reveal lateral resistivity contrasts well, but for quantitative depth modeling it depends on constraining information more than MT due to the lack of electric field measurements in ZTEM. One way to provide this information can be through inclusion of MT data within a joint inversion workflow.

Shallow resistivity variations (down to ca. 500m depth) are imaged with slightly more contrast and detail with the contribution of ZTEM, compared to MT alone. Its contribution to improve deeper imaging by defining shallower variation has not been investigated and can't be assessed with the data at hand, due to lack of deeper anomalies here, but this effect is presumed to be rather marginal.

For MT data sets with good 3D coverage the addition of the more continuous but limited bandwidth ZTEM data introduces only a minor benefit with respect to the MT single domain result. For MT data sets that include magnetic tipper transfer functions the redundancy increases, and the benefit of adding ZTEM is further reduced. Alumbaugh (2016) and Wannamaker (2014) demonstrated in 2D that inclusion of only a few MT soundings in a joint workflow can reduce the uncertainty in ZTEM modeling considerably by calibrating resistivities. An extension of our study could examine this in the 3D case using observed data, with the expectation of a confirmation of the statement also for 3D.

In summary, a ZTEM survey appears to give little contribution to a broadband MT data set of reasonable areal coverage, whereas sparse MT combined with ZTEM is expected to be mutually more beneficial.

REFERENCES

Alumbaugh, D., Huang, H., Livermore, J., and Velasco, M.S., 2016, Resistivity imaging in a fold and thrust belt using ZTEM and sparse MT data: First Break, 34, 65-72.

Caldwell, T.G., Bibby, H.M., and Brown, C., 2004, The magnetotelluric phase tensor: Geophysical Journal International, 158, 2, 457-469.

Holtham, E., and Oldenburg, D.W., 2010, Three-dimensional inversion of MT and ZTEM data: Society of Exploration Geophysicists Annual Meeting, Denver, 655-659.

Hübert, J., Lee, B.M., Liu, L., Unsworth, M.J., Richards, J.P., Abbassi, B., Cheng, L.Z., Oldenburg, D.W., Legault, J.M., and Rebagliati, M., 2016, Three-dimensional imaging of a Ag-Au-rich epithermal system in British Columbia, Canada, using airborne z -axis tipper electromagnetic and ground-based magnetotelluric data: Geophysics ,81(1), B1-B12.

Lee, B., Unsworth, M.J., Hübert, J., Richards, J., Legault, J.M., 2017, 3-D Joint Z-axis Tipper Electromagnetic and Magnetotelluric Inversion: A case study from the Morrison porphyry Cu-Au-Mo deposit, British 2 Columbia, Canada: Accepted for publication in Geophysical Prospecting.

Legault, J.M., Lombardo, S., Zhao, S., Clavero, J., Aguirre, I., Arcos, R., and Lira, E., 2012, ZTEM airborne AFMAG EM and ground geophysical survey comparisons over the Pampa Lirima Geothermal Field in Northern Chile: Geothermal Research Council Annual Meeting, Reno (NV), Transactions, 36, 1001-1008.

Sasaki, Y., Yi, M.-J., and Choi, J., 2014, 2D and 3D separate and joint inversion of airborne ZTEM and ground AMT data: Synthetic model studies: Journal of Applied Geophysics, 104, 149–155.

Sattel, D., and Witherly, K., 2015, The 3D joint inversion of MT and ZTEM data: 24th International Geophysical Conference and Exhibition, Perth, Western Australia.

Soyer, W., Mackie, R., Hallinan, S., Pavesi, A., Nordquist, G., Suminar, A., Intani, R., and Nelson, C., 2017, Multi-Physics Imaging of the Darajat Field: Accepted for presentation at the Geothermal Research Council Annual Meeting, Salt Lake City (UT), Transactions, 41.

Soyer, W., 2002, Analysis of geomagnetic variations in the Central and Southern Andes: PhD thesis, Free University Berlin.

Stark, M.A., Soyer, W., Hallinan, S., and Watts, M.D., 2013, Distortion effects on magnetotelluric sounding data investigated by 3D Modeling of high-resolution topography: Geothermal Research Council Annual Meeting, Las Vegas (NV), Transactions, 37, 521-527.

Legault, J.M., Lombardo, S., Zhao, S., Clavero, J., Aguirre, I., Arcos, R., and Lira, E., 2012, ZTEM airborne AFMAG EM and ground geophysical survey comparisons over the Pampa Lirima Geothermal Field in Northern Chile: Geothermal Research Council Annual Meeting, Reno (NV), Transactions, 36, 1001-1008.

Wannamaker, P.E., and Legault, J.M., 2014, Two-dimensional joint inversion of ZTEM and MT plane-wave EM data for near surface applications: Symposium on the Application of Geophysics to Engineering and Environmental Problems, Boston, Expanded Abstracts, 18-23.

Watts, M.D. and Mackie, R., 2012, Detectability of 3-D sulphide targets with AFMAG: SEG Technical Program Expanded Abstracts, 1-4.

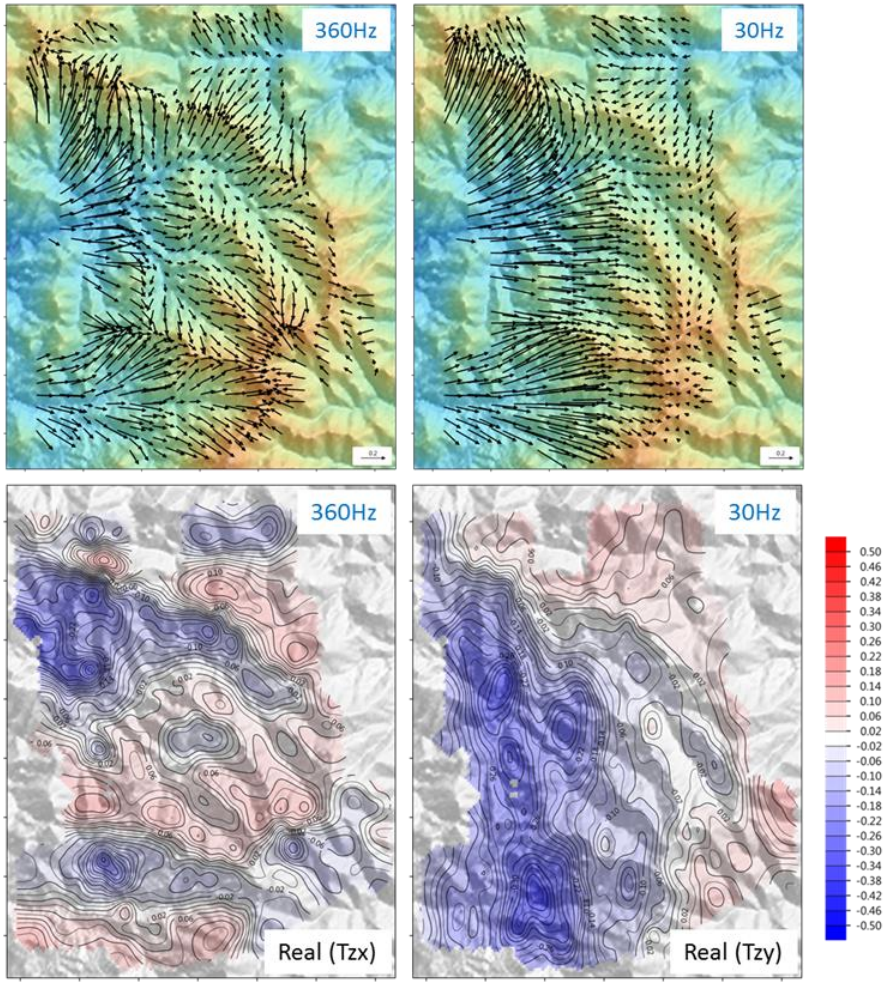

Figure 6: ZTEM data at 30Hz and 360Hz over shaded relief. Top: induction vectors (real parts, convention pointing towards conductors). Bottom: gridded components, NS (left, at 360Hz) and EW (right, at 30Hz).

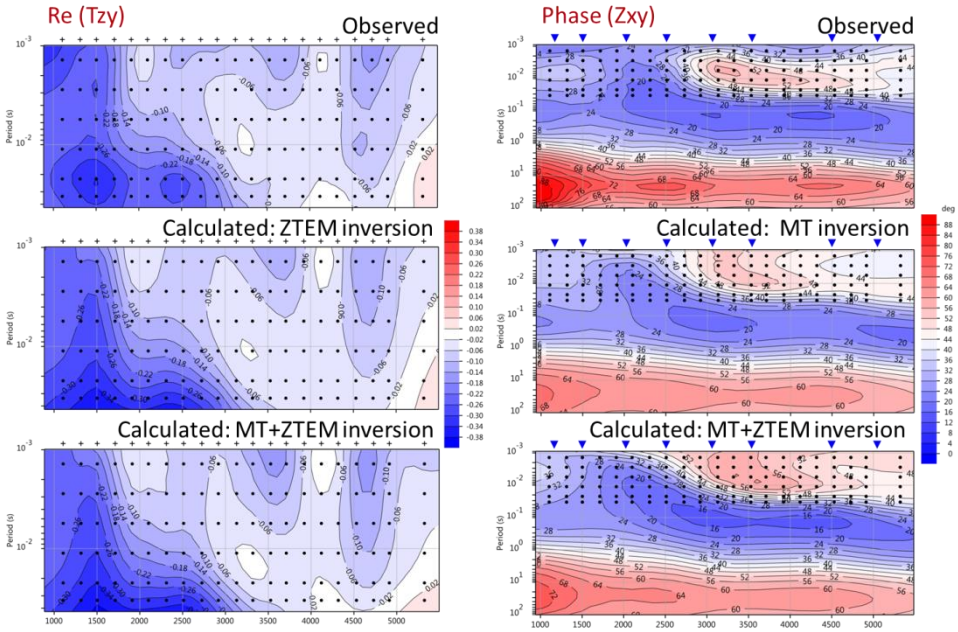

Figure 7: Data fit for 3D inversions along profile "WE" for ZTEM – real part of Tzy, left – and MT data – impedance phase, XY component, right. Top to bottom: observed, single domain inversion, joint MT+ZTEM inversion. Points show ZTEM data.

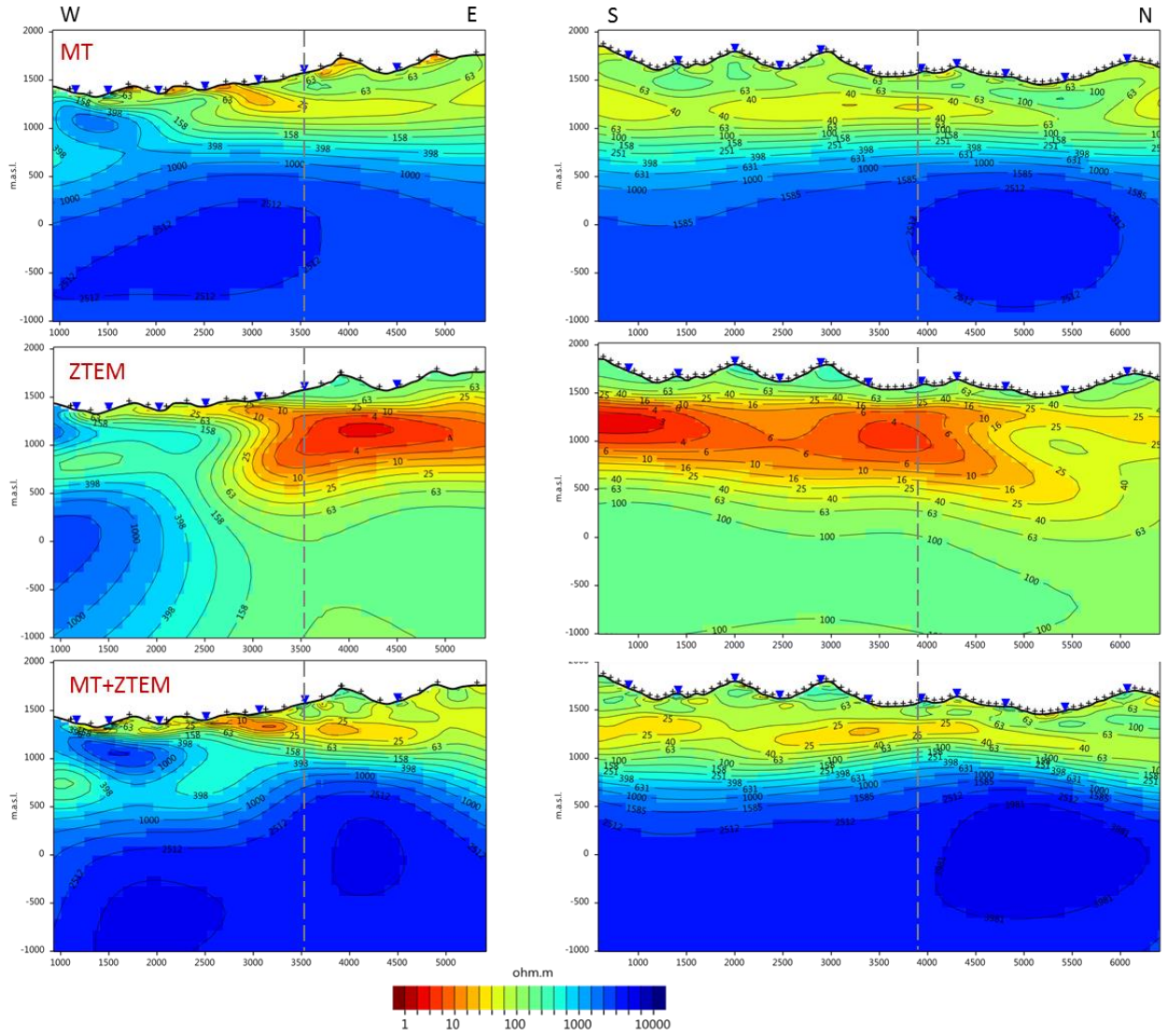

Figure 8: 3D inversion results along profile "WE" (left) and "SN" (right): MT, ZTEM, and joint M+ZTEM (top to bottom). The dashed grey line marks the intersection of the profiles.